Journal of Environmental Chemical Engineering 10 (2022) 108440

Contents lists available at ScienceDirect

Journal of Environmental Chemical Engineering

journal homepage: www.elsevier.com/locate/jece

Scalable synthesis of SWCNT via CH_4/N_2 gas: The effects of purification on photocatalytic properties of CNT/TiO_2 nanocomposite

Sakineh Ghasemzadeh [a], Hassan Hosseini-Monfared [b,*,1], Massomeh Ghorbanloo [a], Thi Hai Yen Beglau [c], Lars Rademacher [c], Alex Spieß [c], Dennis Woschko [c], Christoph Janiak [c]

[a] Department of Chemistry, University of Zanjan, 45195-313 Zanjan, Iran
[b] Department of Chemistry, Amirkabir University of Technology, Tehran, Iran
[c] Institut für Anorganische Chemie und Strukturchemie, Heinrich-Heine-Universität Düsseldorf, 40204 Düsseldorf, Germany

ARTICLE INFO

Editor: Dr. G. Palmisano

Keywords:
SWCNT
Catalytic CVD
Purification
Photocatalysis
SWCNT/TiO_2 composites

ABSTRACT

Single-walled carbon nanotubes (SWCNT) were synthesized by a catalytic CVD method over Mo–Fe–MgO and Mo-Fe-Al_2O_3 catalysts. A systematic investigation was carried out for the purification of SWCNTs by using 20 methods including different acids, acid concentrations, temperatures, and treatment times. The method of consecutive HCl treatment, air oxidation, and second time HCl treatment was successful for the purification of SWCNTs. The purification was effective in the removal of the catalyst support, embedded metal catalysts and non-nanotube carbon materials from the as-synthesized SWCNTs. Effects of purification of SWCNTs on the photocatalytic activity of CNT-based nanocomposites were then studied. The composite SWCNT/TiO_2 containing 15 wt% purified SWCNT was synthesized which showed the maximum photocatalytic activity in the degradation of the dye rhodamine B under optimized conditions. The photocatalytic activity of the composite pure-SWCNT/TiO_2 was much higher than those of non-purified-SWCNT/TiO_2 and neat TiO_2. Overall, this work could clarify the scalable synthesis of SWCNTs, an effective purification method for SWCNTs prepared by CCVD and the purity effect on the photocatalytic activity of CNT-based nanocomposites for wastewater treatment.

1. Introduction

Carbon nanotubes (CNTs) exhibit a unique combination of electronic, thermal, mechanical, and chemical properties [1] which can be useful in many applications, such as catalysis [2], as photocatalysis in composites for water purification [3], in drug delivery and bone scaffolds [4]. Furthermore, single-walled carbon nanotubes (SWCNTs) show chirality-dependent optoelectronic properties [5], suitable for neuromorphic devices [6] and enantiomer-recognition sensors [7]. Of the current methods for the preparation of CNTs, catalytic chemical vapor deposition (CCVD) is an economical synthesis method due to its higher degree of control on the synthesis parameters and its scalability [8]. However, the purity of the synthesized CNTs is lower than from laser ablation or arc discharge methods. The impurities affect the properties of CNTs as a result of forming a composite with CNTs [9]. In general, the main impurities from the CCVD synthesis methods are catalyst supports, metal catalysts, carbonaceous impurities such as amorphous carbon, fullerene molecules, and carbon nanoparticles [10]. Finding a reliable purification protocol for SWCNTs is still a great challenge, since the necessary protocol depends on many factors including the CNT class (single or multi wall carbon nanotubes), surface and structure (existence of defects, whether or not they exist in bundles, diameter), the impurity type and their morphology (particle size, defect, curvature, the number and crystallinity of carbon layers wrapping metal particles), and the purity analysis strategy.

Usually, CNT purification is achieved using wet chemical oxidation or physical methods like filtration. In purifications of CNTs by a wet chemical method, metallic impurities are dissolved in acids and carbonaceous impurities are oxidized at a faster rate than CNTs. Alternatively, gas phase oxidation is a simple method that mainly removes carbonaceous impurities and opens the caps of CNTs with introducing small sidewall defects, but metal catalysts and large graphite particles cannot be removed this way. Therefore, acid treatment is always inevitable for the purification of SWCNTs synthesized by CVD methods to remove metal catalyst and support impurities. In addition, the higher curvature of the graphene sheet of SWCNTs make them easily oxidizable with

* Corresponding author.
E-mail addresses: hahomonfared@gmail.com, hh.monfared@aut.ac.ir (H. Hosseini-Monfared).
[1] ORCID ID: 0000-0001-9157-8198.

https://doi.org/10.1016/j.jece.2022.108440
Received 7 June 2022; Received in revised form 5 August 2022; Accepted 12 August 2022
Available online 19 August 2022

respect to MWCNTs [11]. The presence of metal impurities catalyzes the low-temperature oxidation of SWCNTs [12]. Therefore, strategies, that selectively oxidize carbonaceous impurities and remove metal particles before gas phase oxidation and cause the oxidant gas to homogeneously contact SWCNT samples, are urgently required to obtain high-purity CNTs on a large scale [13]. Hu et al. studied the effects of HNO_3 concentration and the time of reflux on the purification of SWCNTs [14]. They found that nitric acid destroys SWNTs to produce amorphous carbon while reducing the amount of transition metal catalyst remaining in the sample. Furthermore, Martınez et al. proved that treating SWCNTs with hot HNO_3 leads to an efficient elimination of metal impurities and amorphous graphitic platelets [15]. However, additional amorphous carbon nanoparticles are also formed that cover the remaining smaller bundles of CNTs due to intercalation of nitric acid molecules into the CNT bundle structure. This results in the CNT bundle exfoliation and etching of the carbonaceous material [16]. Thus, in order to eliminate amorphous carbon, the nitric acid-treated material has to be annealed to 900 °C [15]. Yang et al. achieved a more rapid oxidation of the C═C double bonds in the thinner tubes into graphene fragments due to the higher chemical reactivity and by this protocol enriched the large-diameter SWNTs by using a concentrated H_2SO_4/HNO_3 treatment [17]. Kruusenberg et al. used different acids for the purification and investigated the effects of metal catalyst impurities of CNTs on their electrocatalytic properties for oxygen reduction. They observed that acid-treated CNT-modified glassy carbon (GC) electrodes showed less catalytic activity for oxygen electroreduction than pristine CNTs because of the absence of metal catalysts on the surface of purified CNTs [9]. Majority of the studied purifications methods are achieved on the CNTs which prepared by electric-arc [14,15] or laser ablation method [16]. Furthermore, only one or a few methods have been examined for the purification of CNTs prepared under the same conditions.

The purpose of this research was to synthesis SWCNT by a scalable CVD method, systematically study the purification of SWCNTs and evaluate the effect of purification on the photocatalytic activity of SWCNT/TiO_2 nanocomposites in the degradation of organic pollutants in wastewater. There are studies on improving the photocatalytic activity of CNT/TiO_2 composite [18,19]. However, to the best of our knowledge there is no systematic study on the effect of SWCNT purity on the photocatalytic activity of SWCNT/TiO_2 nanocomposite. There are various procedures to remove the catalyst metals and non-nanotube carbons from the synthesized CNTs, but different methods for synthesizing CNTs necessitate their own purification strategy. In this study, by examining 20 reported purification methods, we show explicitly the difficulty and at the same time importance of finding a reliable purification strategy for SWCNT prepared by CCVD method. In addition, the SWCNT/TiO_2 composite capability for the elimination of RhB in different conditions was studied by optimizing the weight ratio of SWCNT in x-SWCNT/TiO_2, dosage of photocatalyst 15-SWCNT-TiO_2, concentrations of RhB and pH and the main active intermediates in the photocatalytic process were determined.

2. Experimental section

2.1. Materials and characterization

Titanium(IV) isopropoxide (TTIP) as the TiO_2 precursor, rhodamine B (tetraethylrhodamine, RhB), absolute ethanol and other chemicals were of analytical reagent grade provided by Merck and used without further purification. Deionized water (DI-H_2O) was used for all experiments. As reference, a TiO_2 sample was prepared by a reported procedure [20]. This TiO_2 material is a porous powder consisting of mainly anatase with a BET surface area of about 155 $m^2\ g^{-1}$ and an average crystallite size of 7.1 nm, calculated by Scherrer equation [21]. UV–vis spectra of the solutions were run on an Analytic Jena Specord 210 Plus spectrophotometer. Solid-state light absorptions in UV and visible ranges were studied by UV–visible diffuse reflectance spectroscopy (UV–vis DRS; AvaSpec-ULS2048LTEC). Fourier transform infrared (FTIR) spectra were taken using a Thermo Scientific Nicolet iS10 FTIR spectrometer. Powder X-ray diffraction patterns were collected at a Bruker D2 Phaser, with Cu-Kα radiation ($\lambda = 1.54182$ Å), 30 kV, 10 mA. Measurements have been conducted in the X-ray fluorescence reduction mode to reduce the background intensity caused by the X-ray fluorescence of iron. Transmission electron microscopy (TEM) was performed with a FEI Tecnai G2 F20 electron microscope operated at 200 kV accelerating voltage and images were collected with a Gatan UltraScan 1000 P detector. TEM samples were prepared by drop-casting the diluted material on 200 μm carbon-coated copper grids. Alternatively, TEM images were generated by an EM 208 S, Philips (100 KV, Netherland) electron microscope. GC-MS was used to characterize the GC-detectable products from the RhB degradation under optimized UV/Catalyst/pH/H_2O conditions. GC-MS samples were prepared by the extraction of the organic compounds from aqueous solution with CH_2Cl_2 and injected after concentration on an Agilent GC system 7890B coupled with an Agilent 5977 A mass spectroscopy. N_2 isotherms were measured on a Quantachrome Autosorb 6 for determining the surface area by the Brunauer-Emmett-Teller (BET) method. Samples were degassed on a Quantachrome Flovac at 120 °C for at least 3 h until a pressure below 20 mTorr was achieved. Raman spectra of the SWNT powder were recorded with a Bruker MultiRAM-FT Raman spectrometer equipped with a Nd: YAG-laser. The excitation wavelength of the laser was 1064 nm. The spectra were measured for 200 scans with a laser intensity of at least 15 mW (up to 100 mW). X-ray photoelectron spectroscopy (XPS) measurements were carried out on an ULVAC-PHI VersaProbe II microfocus X-ray photoelectron spectrometer equipped with a polychromatic aluminum Kα X-ray source (1486.8 eV). Binding energies were calibrated to the C1s orbital with a binding energy of 284.8 eV. Experimental XP spectra were fitted by the CasaXPS program, Casa Software Ltd. Thermogravimetric analysis (TGA) was performed on a Netzsch TG 209 F3 Tarsus, with a heating ramp of 5 K min^{-1} under a synthetic air flow up to a temperature of 1000 °C.

The presence of metals in the purified residue was analyzed by an ICP-OES Spectro Arcos spectrometer.

2.2. Synthesis of catalyst **1** (Fe-Mo/Al_2O_3)

This catalyst was prepared by the coprecipitation method [22]. 1.362 g of neutral aluminum oxide (Type 507, Fluka) was dispersed in 20.0 mL of DI-H_2O. Then, the yellow-orange solution of 0.0295 g $(NH_4)_6Mo_7O_{24}4\ H_2O$ and 0.167 g $Fe_2(SO_4)_3$ in 70 mL of DI-H_2O was added to the dispersion of alumina and stirred for 2 h at room temperature. The molar ratio for Fe:Mo:Al_2O_3 was 1:0.2:32. The solvent was evaporated and the resulting solid heated at 90 °C for 3 h. The solid was ground to a fine powder and calcinated at 500 °C for 1 h. Yield 1.43 g.

2.3. Synthesis of catalyst 2 (Fe-Mo/Al_2O_3)

Catalyst **2** was synthesized using the same procedure as for catalyst **1**. All steps in the methods were the same except that the amount of neutral aluminum oxide (Type 507, Fluka) was 0.681 g. The molar ratio for Fe:Mo:Al_2O_3 was 1:0.2:16. By hoping for an easier purification of the later-synthesized, catalyst **2** was synthesized by decreasing the support Al_2O_3 amount to half with respect to catalyst **1**. Yield 0.77 g.

2.4. Synthesis of catalyst 3 (FeMo/MgO)

Following a reported procedure [23], 10.0 g of magnesium nitrate $(Mg(NO_3)_2\ 6\ H_2O)$, 0.070 g of ammonium molybdate $((NH_4)_5Mo_7O_{24}\ 4\ H_2O)$, 3.66 g of citric acid $(C_6H_8O_7\ H_2O)$, and 1.600 g of iron nitrate (Fe $(NO_3)_3\ 9\ H_2O$) were dissolved under vigorous stirring in a minimum amount of deionized water. The molar ratio of Fe:Mo:MgO was 10:1:100. The mixture was refluxed for 6 h at 90 °C and then the resulting solution dried at 150 °C for 15 h. The obtained yellow fluffy

solid was ground well using a mortar and pestle and calcinated at 550 °C for 30 min. Yield 1.60 g.

2.5. Synthesis of SWCNTs

A modified method of Zheng was used for the synthesis of SWCNTs [24] by the catalytic CVD method using the experimental setup shown in Fig. 1. Typically, 0.20 g of the catalyst (**1**, **2** or **3**) was uniformly placed into an alumina boat which was inserted in the center of a 60 mm-diameter quartz tube mounted in an electric furnace. The alumina boat containing the catalyst was heated up to 1000 °C under N_2 flowing at 60 sccm (standard cubic centimeter per minute). In raising the temperature, a N_2 flow was initiated in the quartz tube in order to purge the air from the reaction chamber. The synthesis reaction started by flowing CH_4 at 160 sccm over the catalyst in addition to N_2 (60 sccm) at 1000 °C for 30 min. After stopping the methane, the reactor was cooled down to room temperature under nitrogen. Methane gas as carbon source undergoes pyrolysis reaction and forms vapor carbon atoms which bind to the catalyst and join to each other and grow as single-walled carbon nanotubes (SWCNTs). The obtained SWCNTs were further purified to get the pure form of CNTs. For simplicity, the prepared SWCNTs are denoted according to the catalyst support used for their synthesis: SWCNT-A and SWCNT-M, for alumina- and magnesia originated CNTs, respectively.

2.6. Purification of SWCNT

Various methods used for the purification of as-synthesized SWCNT-A and SWCNT-M are summarized in Tables 1 and 2, respectively.

Method (a): The as-synthesized SWCNTs (0.15 g) were added to 15 mL of a solution of NaOH (3 mol/L) and refluxed for 6 h at 100 °C, and then after separation and washing added to 15 mL of analytical grade 65 wt% HNO_3 and refluxed for 1 h at 150 °C [25]. Thus SWCNT-(a) was obtained. Method (b): 50 mL of 3 mol/L NaOH (100 °C, 6 h) then 7 mL of 37% HCl (100 °C, 8 h) [26]. Method (c): 17 mL of 2 mol/L HCl (25 °C, 24 h) [27]. Method (d): 15 mL of 2 mol/L HCl (25 °C, 24 h) then 5.0 mL of HNO_3:H_2SO_4, 1:3 v/v (60 °C, 5 h) [27]. Method (e): 15 mL of 32% HCl (70 °C, 12 h) then 15.0 mL of 10 mol/L HNO_3 (83 °C, 3 h) [27]. Method (f): 15 mL of 65% HNO_3 (83 °C, 12 h) [28]. Method (g): 11 mL of 6.25 mol/L NaOH (190 °C, 4 h) then 9.33 mL of 3 mol/L HNO_3 (60 °C, 15 min) finally sonication (2 h) [29]. Method (h): Typically, 0.15 g of the as-synthesized SWCNT and 11 mL NaOH (12.5 mol/L) were treated for 4 h at 190 ℃ in a Teflon lined autoclave. After cooling the reaction mixture to room temperature, it was washed several times with portions of 10 mL of DI-H_2O, centrifuged (4000 rpm, 15 min), to set the pH to 7 and dried for 24 h at 90 ℃. For further purification, 0.018 g of SWCNT was refluxed with 4.2 mL of HNO_3 (3 mol/L) for 15 min at 60 ℃. This was followed by sonication in an ultrasound bath for 2 h. Then the mixture was washed with DI-H_2O until the filtrate became neutral and dried at 150 ℃ for 4 h [30].

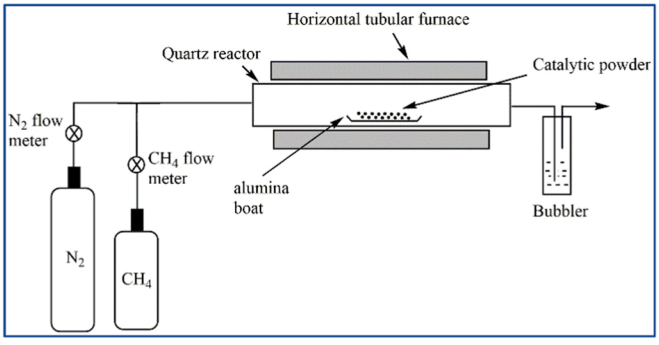

Fig. 1. Schematic diagram of the experimental setup for thermal catalytic CVD synthesis of CNTs. Typical growth temperature is 1000 °C. The CH_4 gas inlet pressure as measured by the gauge is 5 bar. Volume flow rate through the 60 mm quartz tube is CH_4 at 160 sccm and N_2 at 60 sccm.

Table 1
Acid or alkali solution reflux procedures used for the purification of as-synthesized SWCNT-A on catalysts **1** and **2** (Fe-Mo/Al_2O_3)[a].

Method	First step	Second step	Ref.
(a)	NaOH 3 mol/L, 100 °C, 6 h	HNO_3 65%, 150 °C, 1 h	[25]
(b)	NaOH 3 mol/L, 100 °C, 6 h	HCl 37%, 100 °C, 8 h	[26]
(c)	HCl 2 mol/L, 25 °C, 24 h		[27]
(d)	HCl 2 mol/L, 25 °C, 24 h	HNO_3:H_2SO4, 60 °C, 5 h	[27]
(e)	HCl 37%, 70 °C, 12 h	HNO_3 10 mol/L, 83 °C, 3 h	[27]
(f)	HNO_3 65%, 83 °C, 12 h		[28]
(g)	NaOH 6.25 mol/L, 190 °C, 4 h	HNO_3 3 mol/L, 60 °C, 15 min, sonication 2 h	[29]
(h)	NaOH 12.5 mol/L, 190 °C, 4 h	HNO_3 3 mol/L, 60 °C, 15 min, sonication 2 h	[29]

[a] For the purification, 1.0 g of the as-synthesized SWCNTs were treated by methods (a) to (h). Then the SWCNTs were separated by centrifugation and washed with DI-water until the rinse solution reached pH 6-7, followed by drying at 110 °C for 24 h; for further details see the Experimental section.

Table 2
Methods used for purification and functionalization of as-synthesized SWCNT-M on catalyst **3** (FeMo/MgO)[a].

Method	First step	Next steps	Ref.
(i)	HCl 18.5%, 25 °C, 24h	HNO_3 3 mol/L, 60 °C, 15 min, sonication 2h	[23,29]
(j)	HCl 18.5%, 25 °C, 24h	O_2/N_2 1:4 sccm, 450 °C, 2h; HCl 18.5%, 24 h	[23,31, 32]
(k)	Method (j)	HNO_3 65%, 40 min, 85 °C	[33]
(l)	HNO_3 3 mol/L, 16 h, 120 °C	oxidation in air at 550 °C, 30 min	[32]
(m)	HCl 18.5%, 25 °C, 24 h	HCl 18.5%, 25 °C, 24h; HNO_3 3 mol/L, 16 h, 120 °C	[31,32]
(n)	HCl 18.5%, 25 °C, 24h	HCl 18.5%, reflux, 24h; HNO_3 3 mol/L, 16 h, 120 °C; oxidation in air at 550 °C, 30 min	[31,32]
(o)	Sonication in water and reflux at 100 °C, 12 h	HCl 18.5%, 25 °C, 24h; HCl 18.5%, 25 °C, 24h; HNO_3 3 mol/L, 16 h, 120 °C	[31,32, 49]
(p)	HCl 18.5%, sonication 4h	HCl 18.5%, 25 °C, 24h; HNO_3 3 mol/L, 1h, 120 °C	[31,32]
(q)	HCl 18.5%, sonication 4h	HCl 18.5%, 25 °C, 24h; HNO_3 3 mol/L, 1h, 120 °C oxidation in air at 550 °C, 0.5h	[31,32, 49,50]
(r)	Sonication in HNO_3 6M, 4h	H_2SO_4:HNO_3 3:1 v/v, Reflux 2h, 120 °C	
(s)	HCl 18.5%, sonication 4h		
(t)	HCl 18.5%, sonication 4h	HNO_3 3 mol/L, 1h, 120 °C	
(u)	HCl 18.5%, sonication 4h	HNO_3 3 mol/L, 1h, 120 °C; oxidation in air at 550 °C, 0.5h	[19,37, 38,55]

[a] For the purification, 1.0 g of the as-synthesized SWCNTs were treated by methods (i) to (u). Then the SWCNTs were separated by centrifugation and washed with DI-water until the rinse solution reached pH 7, followed by drying at 110 °C for 24 h; for further details see the Experimental section.

Method (i): The as-synthesized SWCNTs on catalyst **3** were refluxed with 14 mL of diluted hydrochloric acid (37% HCl and H_2O (v:v = 1:1) for 24 h to remove the MgO and metal catalyst [23], followed by refluxing with 12.0 mL of HNO_3 (3 mol/L) for 15 min. Finally, the product was sonicated for 2 h [29]. The product was washed with deionized water to neutral pH and then dried at 150 °C for 4 h. Method (j): This method consists of three parts. (Step 1) 14 mL of diluted hydrochloric acid (HCl 37% / H_2O (1:1 v/v) was added to 0.15 g of the as-synthesized SWCNT-M, followed by sonication for 4 min and then stirred at room temperature for 24 h [31]. After washing with DI-H_2O

until neutralization, the product was dried for 24 h at 110 ℃. (Step 2) In the second step, the purified nanotubes were oxidized in air to remove the remaining impurities and amorphous carbon. 0.1468 g of the product obtained in the first part was placed in a boat and heated under the flow of oxygen (50 sccm) and nitrogen (200 sccm) mixture (1:4 vol ratio of O_2/N_2) at 450 °C for 2 h [32]. (Step 3) to remove the metal catalyst nanoparticles that were un-covered by the oxidation process, 0.13 g of the product of the step (2) was treated with 14 mL of diluted hydrochloric acid (HCl 37% / H_2O (1:1 v/v), followed by sonication for 4 min and then stirred at room temperature for 24 h. The product was separated with centrifugation, washed several times with DI-H_2O until the pH equaled to 7, and finally dried for 24 h at 110 ℃ [23]. The purified SWCNT is named SWCNT-(j).

2.7. Functionalization of SWCNTs

For reaction with the TiO_2 precursor titanium tetraisopropoxide (TTIP) to give the SWCNT/TiO_2 composites it is required to modify the surface of CNTs by functionalization [33]. Functionalization also helps for dispersing the prepared CNTs in water. For functionalization of carbon nanotubes with oxygenated functionalities, 1.0 g of purified SWCNT-(j) was refluxed in 50 mL of HNO_3 (65%) for 40 min at 85 ℃. The resulting black product was separated with centrifugation, washed five times with DI-H_2O to remove acid, and finally dried at 105 ℃ for 18 h. The purified and functionalized SWCNT is named SWCNT-(k).

2.8. Synthesis of TiO_2 nanoparticles

Titanium tetraisopropoxide (TTIP, Merck 97%) (0.0328 mol) was first diluted in 5.75 mL of absolute ethanol, molar ratio of EtOH/TTIP = 3, and then added dropwise to 35.46 mL of DI-H_2O. The mixture was stirred for 1 h at room temperature and then placed in a sonication bath for 2 h to improve the formation of white $Ti(OH)_4$ precipitates. TTIP was further hydrolyzed by aging at room temperature for 24 h. Water and alcohol of the resulting gels were then removed by heating for 24 h at 100 ℃. Finally, the obtained xerogel was ground to fine powders and calcined at 400 ℃ for 1 h [20].

2.9. Synthesis of SWCNT/TiO_2

Nanocomposites of SWCNT/TiO_2 were prepared with different weight ratios of SWCNT and TiO_2 [34]. Nanocomposites are denoted as x-MWNT/TiO_2, where x (0.4, 0.8, 2, 3, 8, 15, and 20) represents the SWCNT weight percent in the composite; for example, 15-SWCNT/TiO_2 means 15 wt% SWCNT and 85 wt% TiO_2. For the preparation of 0.8-SWCNT/TiO_2, typically 0.020 g of purified and functionalized SWCNT-(k) was dispersed in 8.9 mL of ethanol by sonication for 15 min. Then 0.033 mol (10.0 mL, 9.31 g) TTIP was added and sonicated for additional 30 min. After that 350 mL of DI-H_2O addition and sonication for 30 min was repeated. The resulting gray product was aged for 20 h at room temperature for completion of the hydrolysis, then the suspension was heated at 100 ℃ for 8 h. Finally, the dried mixture was ground finely and calcined at 400 ℃ for 1 h.

2.10. Photocatalytic properties of the samples

For activity evaluations, RhB was studied as a model compound. The experiments were carried out in an open wide glass photochemical reactor charged with 40 mL of suspension and a magnetic stirrer. Typically, an aqueous suspension was prepared by adding 20 mg of photocatalyst (TiO_2, or SWCNT/TiO_2) powder to 39 mL H_2O and sonicated for 10 min, then 1 mL of 400 ppm RhB solution was added to have a 40 mL solution containing the RhB at 10 ppm concentration and the pH was adjusted to 8.0 with HCl or NaOH as required, and determined with a Metrohm pH meter. The pH value of the 10 ppm RhB solution before the catalytic experiments was 5.83. Prior to irradiation, the dispersions were magnetically stirred in the dark for 30 min to secure the establishment of an adsorption/desorption equilibrium of RhB on the photocatalyst surface. Prior to turning on the lamp, the concentration of the solution was determined, which was considered as initial concentration (c_0) of the RhB solution. The used light was a 30 W UVC fluorescent tube light, which was positioned 5 cm away from the vessel. The temperature of the photocatalytic reaction was maintained at 25 °C. At given irradiation time intervals, the dispersion was sampled (1 mL), diluted to 3 mL by DI water, centrifuged to separate the photocatalyst particles and UV–vis spectra of the photo-reacted solution (measured over the range of 200–800 nm) were recorded using an Analytik Jena Specord 210 Plus spectrophotometer. The spectra were corrected for the baseline, analyzed by comparing the variations of the absorption band maximum (555 nm) in the UV–visible spectra of RhB and the RhB concentration was calculated from the absorbance at 555 nm using a calibration curve.

The reusability of the 15-SWCNT/TiO_2 catalyst was evaluated in five consecutive runs. After each run, the reaction was worked up and catalyst separated by centrifugation, washed with plenty of DI water, and reused in the next photocatalytic reaction run.

Ammonium oxalate (0.1 mM, 0.005 g), t-butyl alcohol (0.5 mL), 0.5 mL methanol, and benzoquinone (0.5 mM, 0.0021 g) as scavengers were introduced into the photocatalytic process to capture holes, hydroxyl radicals and superoxide, respectively, when needed to explore the catalytic mechanism [35–38].

3. Results and discussion

3.1. Synthesis

SWCNTs were catalytically synthesized from the decomposition of methane, CH_4 on a bi-metallic Fe-Mo catalyst system supported on Al_2O_3 or MgO (CCVD method). The experimental set up of the CCVD is shown in Fig. 1. To produce CNTs in sizeable quantities, CCVD is considered to be the best for a low-cost and large-scale synthesis of high-quality CNTs [39]. CCVD does not need very high temperature for the synthesis and the produced CNTs contain only low amounts of unwanted forms of carbon [40]. Methane is a suitable carbon source; it does not decompose at temperatures lower than 1000 °C, hence self-pyrolysis which may produce non-nanotube carbon or poisoning of the catalyst does not occur [41]. Additionally, the catalyst particle size and support morphology/surface area are critical factors in SWCNT synthesis by CCVD. The FeMo/MgO (molar ratio 10:1:100) and Fe-Mo/Al_2O_3 (molar ratio 1:0.2:16) catalysts were obtained by a co-precipitation approach [22,23]. These are the most frequently used catalysts for SWCNT synthesis [42]. In comparison to the conventional chemical impregnation, catalysts prepared by the co-precipitation method are efficient for SWCNT growth [43] and lead to a good homogeneous distribution of the active metal nanoparticles over the support. Bimetallic catalysts show higher efficiency than monometallic catalysts in nanotube production. The Mo is a promoter that prevents the agglomeration of the active catalyst phase on the oxide support, improves catalyst activity and lifetime, and decreases the activation energy for decomposition of the carbon source during the synthesis of CNTs [8].

The type of the produced SWCNTs depends strongly on the nature and texture of the catalyst support. Supports with higher porosity enhance the growth of SWCNTs through the formed metal nanoclusters with 2–10 nm-dimensions [44]. Al_2O_3 as catalyst support is inexpensive, provides good yields for CNT and fluidization behavior [45], however it is hardly removed upon purification [46]. On the other hand, a MgO support is simply removed by acid treatment [47].

3.2. Purification

To date, a number of purification methods have been developed. However, in the preparation of SWCNTs by CCVD methods, the quantity,

morphology and structure of the impurities are specific to each synthesis method and the reaction conditions. Therefore, there is no standardized method for the purification of CNTs which are synthesized differently [48]. Actually, the features of the crude CNTs require their own specific purification strategy to achieve high quality CNTs with the desired properties for the subsequent applications. To find a suitable purification method for our SWCNTs, we have tried first acid or alkali solution reflux procedures reported in the literature for the purification of SWCNTs [10]. The as-synthesized SWCNTs were dispersed in an acid or NaOH solution using sonication. After each treatment step, the reaction products were washed with plenty of DI-water until the filtrate was neutral in order to remove the generated reaction products which may coat the surfaces of the nanotubes. The acid or alkali solution reflux procedures examined for the purification of our as-synthesized SWCNTs by the Fe-Mo/Al_2O_3 catalysts are summarized in Table 1. In summary, reflux in dilute NaOH solution, concentrated HNO_3, concentrated HCl, HNO_3/H_2SO_4, and sonication in dilute HNO_3 were not effective for the purification of as-synthesized SWCNTs. Results of the analyses by FTIR, SEM, EDX, and TEM techniques indicated that with neither of these methods the metal catalysts and/or the alumina support were removed completely. In the Electronic Supplementary Information file, Fig. S1 shows TEM images of the as-synthesized SWCNT-A and purified SWCNT-A and Fig. S2 depicts the TGA analysis of the purified and SWCNT-A.

The methods tried for removing the impurities from as-synthesized SWCNT-M are tabulated in Table 2. Different concentrations of HCl, HNO_3, H_2SO_4/HNO_3, different treatment time, various temperature and/or sonication were tried. While disentanglement of the carbonaceous and catalyst impurities from the CNTs is an important step in the acid reflux procedure, the purification task was completed with plenty of DI-water washing to separate the impurities from the CNTs. Of the used methods, the method (j) was efficient for the purification of our synthesized SWCNTs on the FeMo/MgO catalyst by the CCVD method. In method (j), the as-synthesized CNTs were treated in 18.5% HCl for 24 h at room temperature to remove the MgO supports and Fe-Mo catalysts first and were then separated through centrifugation and washed several times with DI-water until the filtrate became nearly neutral. After drying at 110 °C for 24 h, the purified nanotubes were then oxidatively treated under a flow of synthetic air (oxygen 50 sccm / nitrogen 200 sccm) gas mixture at 450 °C for 2 h. For a second purification step the resulting material was stirred in 18.5% HCl for 24 h at room temperature. After washing and drying the residue was refluxed in HNO_3 (65%) for 40 min at 85 °C. The resulting product was washed and dried at 105 °C for 18 h to get SWCNT (k). HCl treatment was achieved two times in method (j) since evaluation of the product by TGA (see the next section) showed uncompleted removal of the catalyst and support. The HCl treatment is suitable to remove metal particle impurities.

TEM screening of the purified SWCNT-M just by HCl-reflux, showed the presence of some metal catalysts trapped inside the CNTs. The strategy used in method (j) is consecutively gas phase oxidation by O_2/N_2 to open the carbonaceous shells which encapsulate metal particles, treatment with concentrated HCl to dissolve the metal catalyst particles to get highly pure SWCNT with trace metal. In a similar approach, Ma et al. had developed a method for removing catalytic particles and encapsulating graphitic shells in the purification of SWCNTs [51]. In method (k), functionalization of the purified SWCNT-(j) surface with carboxylates during reflux in concentrated HNO_3, imparts negative charges that facilitate the exfoliation of CNT bundles and increases the solubility in polar media for a colloidal dispersion of CNTs in polar media, such as ethanol and water, for further studies [52,53]. Furthermore, the incorporation of oxygen-containing groups onto the graphitic surface of CNTs leads to enhancement of interfacial adhesion. As a result, the unique mechanical and electrical properties of CNTs can be transferred to the properties of CNT-based composites [54].

The purity and quality of each sample were documented by TGA, Raman, and TEM.

3.2.1. TEM analysis

Fig. 2 shows the TEM images of as-synthesized SWCNT-M. Bundles of SWCNT-Ms span between large agglomerations of amorphous and nanocrystalline carbon and metal nanoparticles similar to the SWCNTs prepared by others [31]. In addition to a mixture of bundles of straight and spiral SWCNTs, there are carbonaceous material (amorphous), gray graphitic particles, and black catalyst (Fe and Mo) grains (Fig. 2A). The catalyst particles are enclosed by SWCNTs or a non-nanotube carbon mat. The length of the as prepared nanotube bundles is about several micrometers. Fig. 2B shows that the carbon matrix is not completely removed by three treatments with HCl-air oxidation at 450 °C for 2 h. However, most of the metal catalysts even encapsulated particles are removed by HCl digestion according to method (j). Elimination of the metal impurities is also confirmed by TGA measurements in the next section. HNO_3 treatment removes most of the amorphous carbon and SWCNTs-(k) are seen very clearly with respect to SWCNT-(j). However, some patchier coating is also seen along with occasional agglomerations, and some tubes appeared clean and uncoated. Fig. 2C shows that SWCNTs are mainly in the form of ropes consisting of individual graphene cylinders in Van der Waals contact. The length of the SWCNTs exhibit no significant change after the functionalization step, due to the short time for concentrated HNO_3 reflux at 85 °C. The TEM images of Fig. 2C show only SWCNTs and nanoparticles, from which we can conclude that the final product is SWCNTs and fine graphitic nanoparticles. The images of the 15-SWCNT/TiO_2 nanocomposite clearly show an intimate contact between very small nanoparticles of TiO_2 and purified/functionalized SWCNTs (Fig. 2D).

3.2.2. XRD analysis

Powder X-ray diffraction was carried out in order to determine possible crystalline impurity phases and to follow the effects of purification treatment on the as-synthesized SWCNTs. Fig. 3 compares powder X-ray diffraction (XRD) patterns of the synthesized FeMo/MgO catalyst, as-synthesized SWCNTs, purified and functionalized SWCNTs by method (k), TiO_2, and the 15-SWCNT/TiO_2 nanocomposite. The XRD analysis of the purified and functionalized SWCNT sample shows the absence of FeMo/MgO reflexes in Fig. 3A [23]. The main observed diffraction peak at $2\theta = 25.9^\circ$ due to the (002) planes confirm the single-walled nature of the synthesized CNTs [55]. In the as-synthesized SWCNTs the MgO reflections, labeled by (*), appear as intense peaks at 37.0 and 42.9° 2θ. In addition, a broad peak at 34.7°, labeled by (◆), can be assigned to the catalyst. Using CVD methodology, the resulting crystalline impurities in the as-synthesized SWCNTs product are mainly amorphous carbon and catalyst particles. The catalyst (support and metal particles) is removed to a large extent by 18.5 wt% hydrochloric acid, method (j). Unsymmetrical appearance of the peak at $2\theta = 25.9^\circ$ shows the participation of amorphous carbons in addition to graphitic CNT. The broad maximum about 24.5° is a typical signature of amorphous carbon. Notably absent is a sharp feature at 27° signaling the absence of graphite, onions, and capsules in significant amounts [56]. Deconvolution of the peak at $2\theta = 25.9^\circ$ showed graphitic-C/amorphous-C ratio equal to 2.22 which increased to 3.82 after purification (Fig. S3). The air oxidation at 450 °C and reflux in concentrated HNO_3 at 85 °C (method (k)) remove some of the amorphous carbon of the as-synthesized SWCNT.

The nanocomposite 15-SWCNT/TiO_2 showed a similar XRD pattern to neat TiO_2 prepared from TTIP in the anatase polymorph (Fig. 3B), and the relatively low intensity diffraction peak at 25.9° 2θ is now covered by the (101) reflection of TiO_2. A signature of the present carbon contribution is the increasing baseline at below 15° 2θ.

The mean crystallite size of the TiO_2 nanoparticles in neat TiO_2 and in the nanocomposite 15-SWCNT/TiO_2, calculated by the Scherrer equation, yielded 7 nm in both cases.

3.2.3. TGA analysis

The quality of CNTs and content of the metal impurity was evaluated

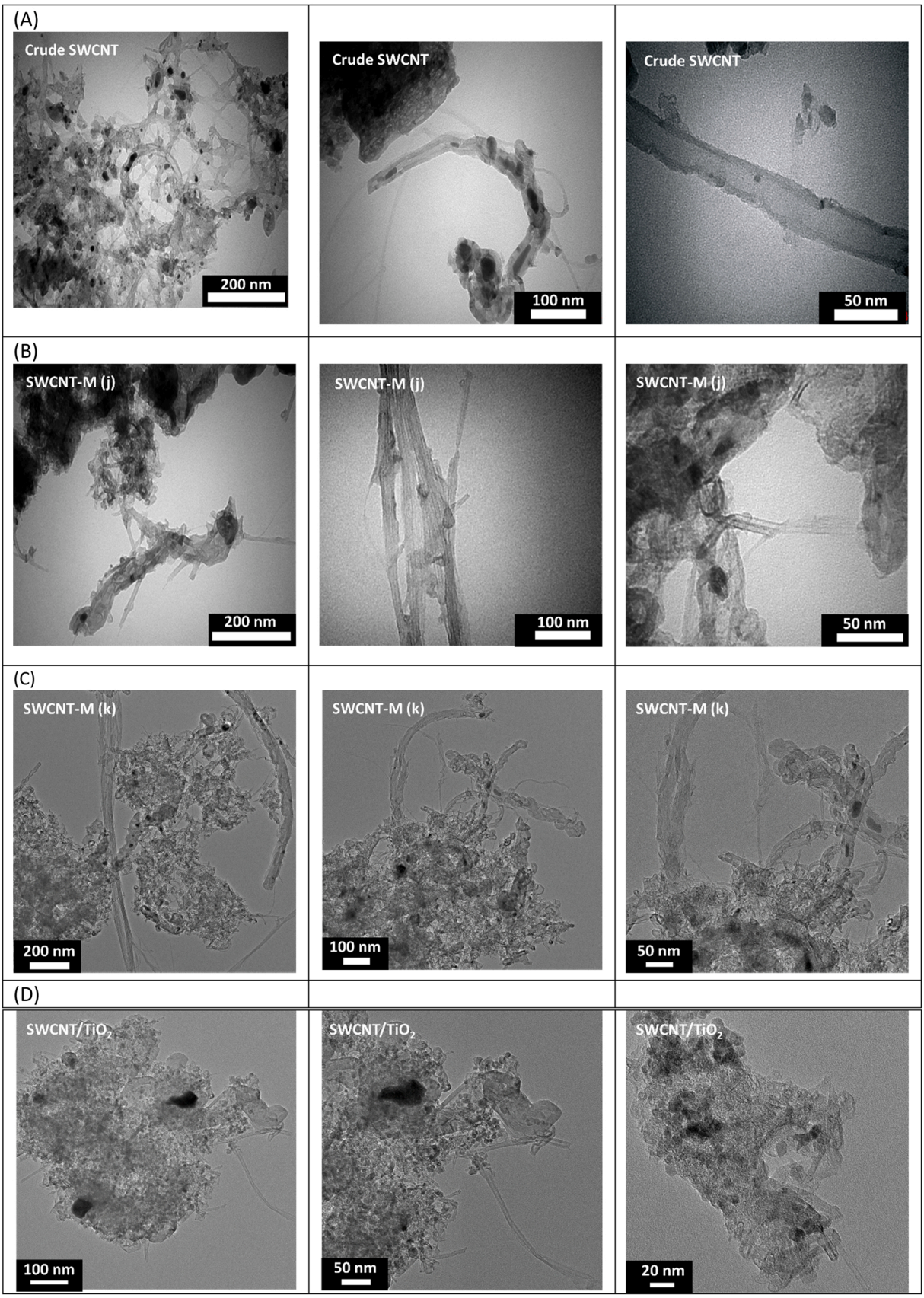

Fig. 2. TEM images of the nanotubes synthesized over the FeMo/MgO catalyst with different magnifications; (a) the as-synthesized SWCNT, (b) the purified SWCNT-M by method (j), (c) images of the purified and functionalized SWCNTs by method (k), and (d) 15-SWCNT/TiO_2 nanocomposite.

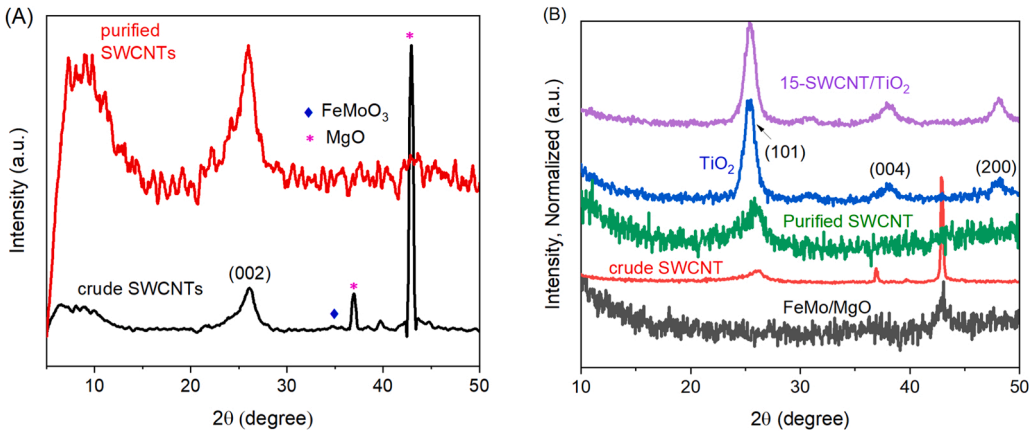

Fig. 3. XRD patterns of (A) FeMo/MgO catalyst, (B) TiO_2, and 15-SWCNT/TiO_2.

quantitatively using TGA by simply combustion of the as-synthesized and purified SWCNT-(k) samples under air. In a 100 sccm air flow, SWCNTs burn between 500 and 700 °C, whereas amorphous carbon gasification occurs between 300 and 500 °C [57]. Usually, purer and less defective CNT samples oxidize at temperatures higher than 500 °C [58]. The TGA data for as-synthesized (crude) SWCNT-M, purified SWCNT-M by method (j), and purified SWCNT-M using method (k) are displayed in Fig. 4. The data for the as-synthesized SWCNTs show a slight increase in mass at low temperatures due to oxidation of the Fe and Mo metal impurities (Fig. 4A); the residual mass after air oxidation was 55.5%. The carbonaceous fractions begin to combust at ~200 °C and are mostly removed by oxidation below 500 °C. So, the SWCNT-M synthesis yield by the catalytic CVD method is about 48%. The treatment by hydrochloric acid solution removes most of the metal and support impurities and residual mass is decreased from 55.5% to 3.7% (Fig. 4B) for purified SWCNT-M using method (j). Further reduction of the residual mass down to 1.4% is seen after treatment of the purified SWCNT-(j) with concentrated HNO_3 according to method (k) (Fig. 4C). The HNO_3 treatment not only removes the remaining metal but also functionalizes the surface of the SWCNTs and non-nanotube carbonaceous fractions with oxygen containing groups [59]. The observation of a black colored filtrate during washing with water and separation with centrifugation (see the Experimental section) confirms that the smaller non-nanotube particles are removed by dispersion in water. Additionally, the 4.5% mass loss up to 500 °C for SWCNT-M(k) is due to the remaining amorphous and functionalized particles. The final purity is evaluated to be > 94% by considering the 4.5% mass loss below 500 °C, and the residual mass of less than 1.5 wt% above 850 °C. The residual mass at 875 °C is related to the oxidized metal impurities (~1.4%). The ICP analyses of the residue showed the metals are Fe 0.3896 wt%, Mg 0.0163 wt% and Mo 0.0241 wt%. The purified CNTs are stable under air (100 sccm) up to 600 °C, Fig. 4. Our TGA results for the purified SWCNT-(k) (T_d = 600 °C) are similar to reported studies in the literature [31,60,61].

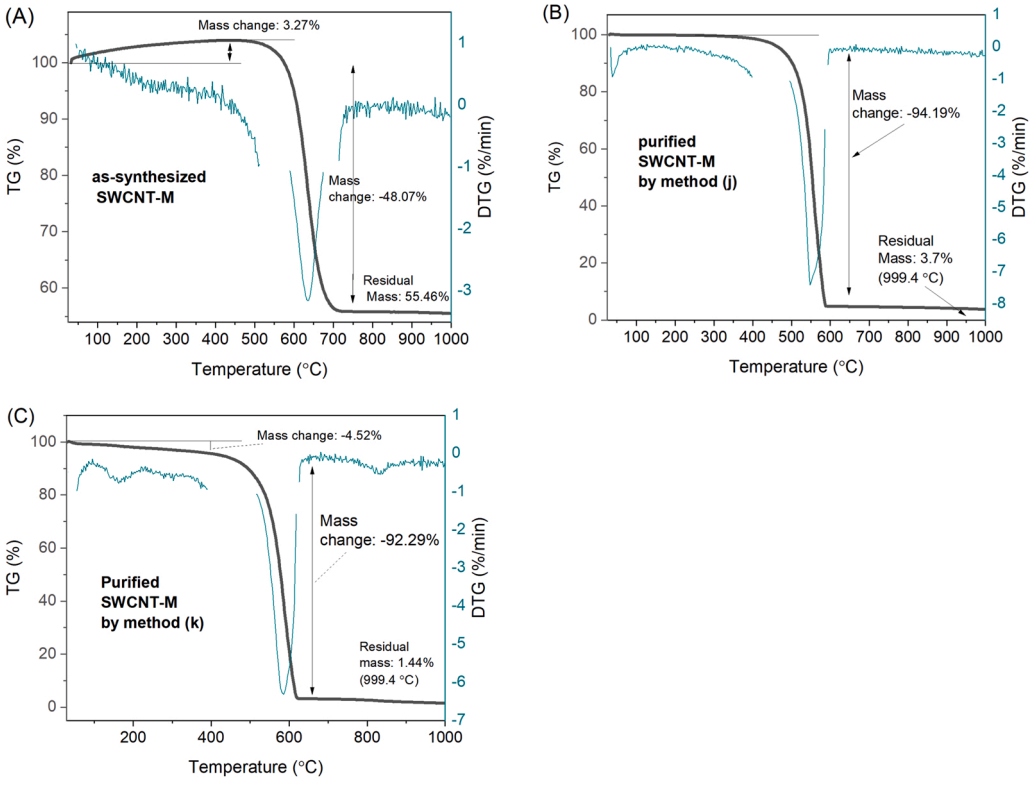

Fig. 4. TGA data under air of (A) as-synthesized SWCNT-M materials, (B) purified SWCNT-M by method (j), and (C) purified SWCNT-M using method (k).

3.2.4. Raman spectral analysis

The Raman spectra of as-synthesized SWCNT and the purified samples by methods (j) and (k) are shown in Fig. 5. The Raman spectra were recorded by exciting the samples with a laser at 1064 nm. The nanotubes with cylindrical symmetry show the Raman peak of crystalline graphite placed at 1591 cm^{-1} (G-band), whereas disordered sp^2 carbon due to the impurities of amorphous or small graphitic particles show broad peaks about 1279 (D-band) *and* at 1591 cm^{-1} (G-band) [62]. The 2D band (2547 cm^{-1}) is the second order harmonic of the D band and presents a measure of crystallinity of the graphitic structures [63]. In addition, as-synthesized SWCNTs show very weak low-frequency radial breathing mode bands centered at 323, 302, 263, and 175 cm^{-1} (not shown). The G-band corresponds to stretching vibrations of sp^2-hybridized carbon atoms and the D-band is associated with disorder-induced symmetry-lowering effects [64]. The acid treatment greatly reduced the diffuse background and nearly eliminates the catalyst peaks (1762 and 1833 cm^{-1}), in agreement with TGA observations. Since the purified and as-synthesized-SWCNTs show only one peak around 1590 cm^{-1} [32], it is suggested that only SWCNTs with the same diameter are produced by our synthesis method. Furthermore, no peaks of fullerene (1400–1500 cm^{-1}) are seen in the Raman spectrum of the crude SWCNTs. The Raman profile equals the spectrum reported by Rao et al. [62]. With the exception of the 1279 cm^{-1} band, all the Raman bands of the crude SWCNTs are substantially reduced in intensity in purified SWCNTs (Fig. 5). The loss in Raman intensity by oxidation does not correspond to destruction of the nanotube structure [65]. The high relative intensity of the low symmetric carbon band at 1279 cm^{-1} to the sp^2 carbon mode at 1591 cm^{-1} indicates a loss of long-range order in purified SWCNT-M(j) and SWCNT-M(k), most likely due to partial conversion of sp^2- to sp^3-hybridized carbon atoms. The I_D/I_G ratio increase and I_{2D}/I_G ratio decrease in the case of SWCNT-M(j) and SWCNT-M(k) compared to as-synthesized-SWCNT-M. The decrease of both ratios indicates a reduction in the crystallinity degree upon air and HNO_3 reflux oxidation, respectively. Besides, the slight intensity decrease in the D band after purification indicates still a substantial presence of carbonaceous impurities of amorphous carbon, whose appearance was above confirmed by XRD, TGA and TEM as well. A similar change in the intensity ratio of these bands was observed for HNO_3-treated [66] and fluorinated [67] SWCNTs.

It is observed that the 2D band has the shape of a perfect Lorentzian with a half-height width of 76 cm^{-1} in crude SWCNT-M, further indicating the presence of single-walled nanotubes only. With an excitation laser at 532 nm, the D-band position shifted (71 cm^{-1}) and appeared at 1350 cm^{-1} (Fig. S4). This is in good agreement with other literature reports for bundled SWCNTs [68].

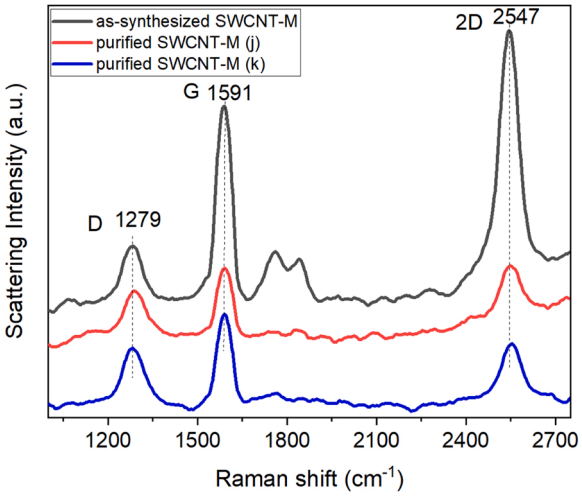

Fig. 5. Raman spectra obtained at 1064 nm for crude and purified materials that were obtained by methods (j) and (k). Crude SWCNT: $I_D/I_G = 0.61$, $I_{2D}/I_G = 1.62$; SWCNT-M(j): $I_D/I_G = 1.15$, $I_{2D}/I_G = 1.01$; SWCNT-M(k): $I_D/I_G = 1.15$, $I_{2D}/I_G = 0.82$.

3.2.5. XPS analysis

X-ray photoelectron spectroscopy (XPS) is a useful tool for assigning the nature of the functional groups and structural defects on the nanotube surface. In addition, by comparing the intensities of different atomic core levels, the overall atomic composition can also be determined, which can yield information on the ratio of SWCNT and TiO_2. Fig. 6A, D, and G represent the XPS survey spectra of SWCNT-(j), SWCNT-(k) and 15-SWCNT/TiO_2 samples. Three XPS peaks were observed for both SWCNTs samples, which correspond to emission from C1s (284.4 eV), the satellite peak of C1s, and O1s. Notably, metal catalyst impurities were not detected in the acid-treated SWCNTs by XPS. The most intense C1s peak at around 284.4 eV (Fig. 6A) is comparable to the C1s binding energy of graphite and is assigned to sp^2-hybridized carbon atoms on the SWCNT walls. A smaller speak at around 284.8 eV is related to sp^3-hybridized carbon atoms and may originate from the presence of defects on the tube walls and/or graphitic platelets [69]. The other small peaks around 286.5, 287.8 and 290.5 eV are assigned to C–O, C═O and π–π * plasmon, respectively [70]. Deconvolution of the XPS O1s peak (Fig. 6C, F and Table S1) confirmed the presence of some C═O and C-OH/C-O-C groups on the CNT surface at 530.7 eV and 532.8 eV, respectively, for SWCNTs-(j) and SWCNTs-(k). The total amount of oxygen on the surface of SWCNTs-(j) and SWCNTs-(k) were 3.5 at% and 3.9 at%, respectively, as detected by XPS measurements. As is evident, there is an increase of oxygen content on the walls of CNTs for HNO_3 treatments attempted here. The HCl is not an oxidation agent, and therefore we can safely assume that the amount of the oxygen found on SWCNTs was produced during the air oxidation treatment at 450 °C and HNO_3 reflux.

The XPS survey spectrum of 15-SWCNT/TiO_2 shows the peaks corresponding to Ti, O, and C, without other element impurities (Fig. 6G). The formation of a C-O-Ti linkage between the SWCNT-carbon and Ti is confirmed by the appearance of a peak at 289.1 eV (Fig. 6H) in the expanded C 1 s region. Fig. 6I shows the high-resolution XPS spectra for the O 1 s region of the composite SWCNT/TiO_2. Two types of oxygen atoms are seen in the O 1 s region. One peak is attributed to Ti–O in the composite, while the other one is assigned to the C-OH (or C-O-C) hydroxyl group. The photocatalytic activity of the composite is enhanced by the increasing hydroxyl content on the surface of the composite due to hydrophilicity improvement [71].

3.2.6. FT-IR analysis

FTIR was conducted on as-synthesized and purified CNTs and their corresponding spectra are shown in Fig. 7. Comparison of the IR transmission spectra of the purified SWCNT-(k) and as-synthesized SWCNT clearly shows the functionalization with oxygen containing groups due to the oxidation (Fig. 7). A broad band centered at around 3480 cm^{-1} and a band at 3129 cm^{-1} can be related to O-H stretching vibrations in C-OH groups and water, respectively; a band at 1729 cm^{-1} is due to C═O stretching vibrations in carboxyl and carbonyl groups [65]. A band at 1619 cm^{-1} corresponds to conjugated C═C stretching. The O-H deformation vibrations in C-OH groups were observed at 1402 cm^{-1}. A weak broad band at 1123 cm^{-1} is associated with C-O stretching vibrations. The positions of the vibrational modes are similar to positions of vibrational modes that appeared in the IR spectrum of as-synthesized SWCNT (Fig. 7A and B); however, the spectrum of the purified SWCNT-M (k) has a carbonyl peak at 1729 cm^{-1}. The peak at 2345 cm^{-1} is associated with the sorption of CO_2 onto the surface of the as-synthesized SWCNT. The hydroxyl stretching (3445 cm^{-1}) and aliphatic hydroxyl bending (1402 cm^{-1}) bands may also result from oxidation during the purification of the as-synthesized SWCNT material and/or ambient atmospheric moisture [29].

The TiO_2 modified with 15% SWCNT was analyzed with FTIR and

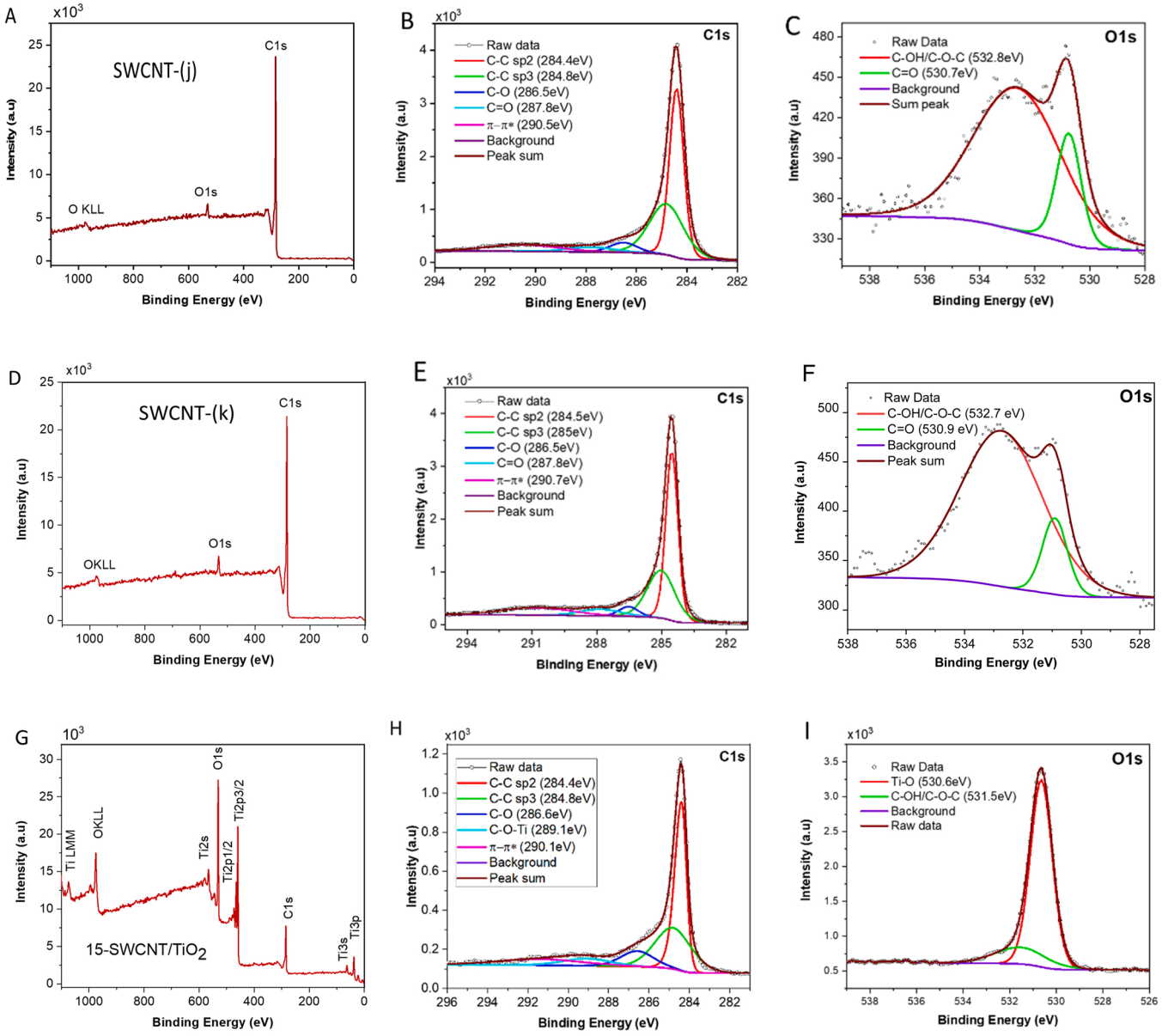

Fig. 6. X-ray photoelectron spectra (XPS) of SWCNT-(j) (A to C), SWCNT-(k) (D to F), and 15-SWCNT/TiO_2 nanocomposite (G to I).

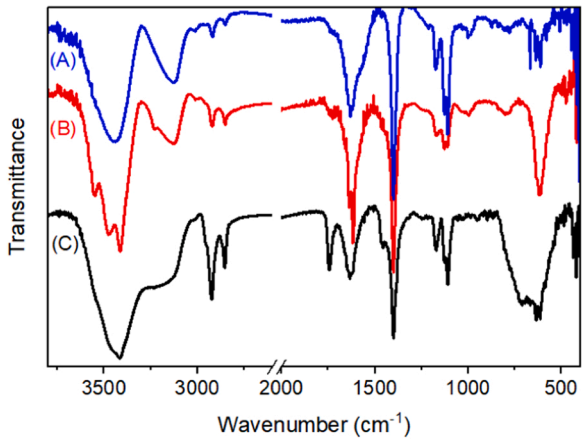

Fig. 7. FTIR transmission spectra of (A) crude SWCNT-M, (B) purified SWCNT-M(k), and (C) 15-SWCNT/TiO_2.

the spectrum is shown in Fig. 7C. The strong and very broad band at 3600 cm^{-1} can be assigned to the hydroxyl groups bound to titanium centers (Ti-OH), the hydroxyl groups of SWCNT, and adsorbed water. Besides, a broad and strong band between 500 and 718 cm^{-1} corresponds to Ti-O bond vibrations [72]. What is interesting to note, comparing the FTIR spectrum SWCNT-(k) with that of 15-SWCNT/TiO_2, is that the C═O vibration of SWCNT-(k) have shifted from 1729 to 1745 cm^{-1} and the C-O stretch from 1123 to 1108 cm^{-1} after the deposition of titania. The C═O mode shift to higher wavenumber and frequency can be explained by the formation of Ti-carboxylate binding upon reaction of Ti-OH with carboxylic acid functional groups of SWCNT-M(k). Furthermore, in 15-SWCNT/TiO_2, the broad and very strong absorption below 800 cm^{-1} of neat TiO_2 shifted toward high wavenumber. This peak is a combination of Ti-O-Ti and Ti-O-C vibrations (798 cm^{-1}) [73]. All these findings show the formation of, at least in part, a chemical bond between titanium and SWCNT-(k). The calcination at low temperature of 400 ℃ for 1 h was used to prevent the decomposition of the SWCNT and transformation of anatase.

3.3. Photocatalytic measurements

The change in photocatalytic degradation of RhB under UV light illumination was followed by UV–vis spectroscopy. First, the material was left in the dark to reach equilibrium and then followed by UV light illumination. Preliminary experiments showed that the adsorption occurs in the first 10–15 min (Fig. S5). However, to ensure a complete reaction the mixture was stirred for 30 min in the absence of light. Hence, additional decrease in the remained RhB concentration under UV light irradiation, after 30 min stirring in dark, results from the photocatalytic degradation of RhB. The photocatalytic activities of x-SWCNT/TiO_2 (x = 0.4–20) were measured by the photodegradation of RhB as model reaction under UV light (366–576 nm), and the results are shown in Fig. 8. The normalized temporal concentration changes (c/c_0) of RhB during the photodegradation were proportional to the normalized maximum absorbance (A/A_0) and derived from the changes in the dye's absorption profile 555 nm at a given time interval. It was clear from Fig. 8 that the 15-SWCNT-TiO_2 (15 wt%) composite showed significant progress in the photodegradation of RhB compared to other composites. We fitted our results of the photocatalytic reaction over the SWCNT/TiO_2 composites to the apparent first-order equation $\ln(c_0/c) = kt$. This indicates that the photocatalytic degradation of RhB follows pseudo-first-order kinetics. Catalytic activity of the composites increased by increasing the SWCNT/TiO_2 mass fraction from 0.4 to 15. Pseudo first order rate constants for 15-SWCNT-TiO_2 (17.68×10^{-3} min^{-1}) and 20-SWCNT-TiO_2 (17.32×10^{-3} min^{-1}) were almost the same (Table S2). The SWCNT/TiO_2 with a mass fraction of 15 wt% showed the highest photocatalytic activity due to highest synergistic effect; with an increase in the first-order rate constant by a factor of 2.0 with respect to 0.4-SWCNT/TiO_2 and neat TiO_2. The 15-SWCNT-TiO_2 nanocomposite was chosen for further studies. As shown in Fig. 8, the slope of the straight line of $\ln(c_0/c)$ versus time for 15-SWCNT-TiO_2 (17.3×10^{-3} min^{-1}) is almost twice of that for TiO_2 (8.9×10^{-3} min^{-1}), which means that the photodegradation rate of RhB using 15-SWCNT-TiO_2 as catalyst is two times that of TiO_2 as catalyst. Therefore, the reaction conditions were optimized by varying the concentrations of 15-SWCNT-TiO_2, RhB, and pH value of the solution.

The effects of dosage of photocatalyst 15-SWCNT-TiO_2, concentrations of RhB and pH on the photocatalytic removal of RhB were studied. The highest photocatalytic degradation rate was achieved for 0.03 g/40 mL dosage of 15-SWCNT-TiO_2 (Fig. S6) and initial concentration of 20 mg/L RhB (Fig. S7). At pH 8, 79% of the initial dye at a concentration of 20 ppm was decomposed by 15-SWCNT-TiO_2 after 60 min under UV light irradiation (Fig. S8).

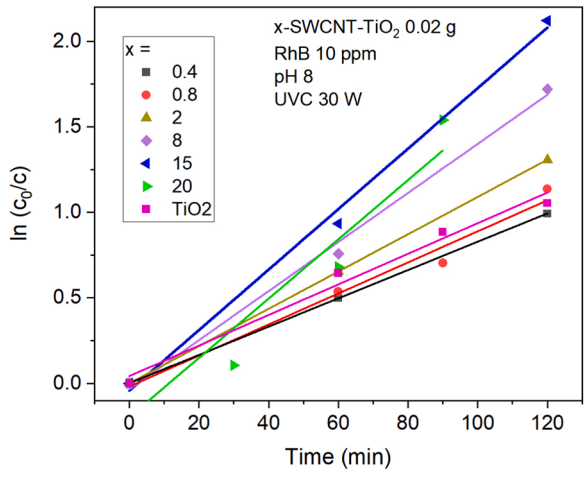

Fig. 8. Photocatalytic degradation of RhB and corresponding kinetic plots for x-SWCNT-TiO_2 composites.

3.3.1. Photocatalyst recyclability

Recyclability is an important factor for practical applications of catalysts [74]. Stability of 15-SWCNT/TiO_2 was studied in the course of consecutive runs for RhB photodegradation to address its prolonged use. The photodegradation of RhB was monitored for four consecutive runs, each for 120 min. After each run, 15-SWCNT/TiO_2 was filtrated and washed thoroughly with plenty of water and fresh RhB solution was added. 15-SWCNT-TiO_2 exhibited high stability and recyclability for the photocatalytic degradation of RhB, which provides great potential for the feasible treatment of organic pollutants (Fig. 9). The total photo-degradation efficiency of 15-SWCNT/TiO_2 reduced about 18% after five cycles, which is attributed to the catalyst weight loss during the recycling process. Results of these experiments proves the cyclic potential of the photocatalyst and its stability provides great capacity for the feasible treatment of organic-dye pollutants of water. Detailed analysis of the results shows that the adsorption of RhB decreases from 66% to 29%, but the photocatalytic efficiency increases from 34% to 52%. The same trends in the photocatalytic activity of the graphene oxide/TiO_2 composite has also been reported [75]. Under dark condition, there is a gradual decrease in the removal of RhB after each cycle in the consecutive runs which is ascribed to the adsorption of RhB on the porous surface of 15-SWCNT/TiO_2. Even though the composite was separated and washed thoroughly with plenty of water at the end of each run and then used in the next experiment, many RhB molecules remain in the 15-SWCNT/TiO_2 composite, leading to the weakening of the next adsorption ability of the used composite. This conclusion is confirmed by the gradual improvement in the photocatalytic efficiency of 15-SWCNT/TiO_2 during the recycle experiment. In comparison with the first run, the number of the photocatalyst active sites and free RhB molecules, which are not trapped in the composite pores, are higher in the next run. Therefore, a gradual increase in the photocatalytic efficiency of 15-SWCNT/TiO_2 is observed after each run. The observed trends in the adsorption in dark and photocatalysis under UV prove that the final removal of RhB from solutions is caused by the photocatalytic degradation rather than the adsorption process. Adsorption of RhB on the photocatalyst led to the saturated photocatalyst.

3.3.2. Identification of active species

To analyze the main active intermediates in the degradation of RhB by 15-SWCNT/TiO_2, the photocatalytic process was studied under optimized conditions in the presence of benzoquinone (BQ) as superoxide radical scavenger, *t*-butyl alcohol (t-BuOH) and methanol as hydroxyl radical scavengers, and ammonium oxalate as hole scavenger

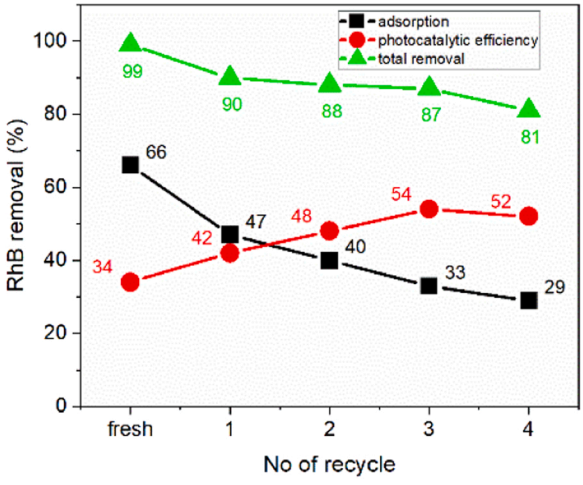

Fig. 9. Adsorption and photocatalytic recycling experiments of 15-SWCNT/TiO_2. Adsorption efficiency was obtained in dark after 30 min stirring. Conditions: total time for adsorption and photocatalytic process 150 min, cat 0.03 g, pH 8, RhB 10 ppm, UVC 30 W.

[35–38,76,77]. The variation of c/c_0 of RhB as a function of irradiation time was studied before and after addition of scavengers into the photocatalytic system. The role of the active species was determined through the variation of c/c_0 of the dyes after the scavengers were added into the photocatalytic system (Fig. S9). Comparison of the results in Fig. S9 shows that hydroxyl radical ($^{\bullet}OH$) is the dominant reactive oxidative species. Therefore, t-BuOH and BQ in the reaction mixture both completely inhibited the photocatalytic degradation of RhB, indicating that the degradation of RhB is mostly achieved by photogenerated hydroxyl ($^{\bullet}OH$) and superoxide anion ($^{\bullet}O_2^-$) radicals; direct oxidation on photogenerated holes is a minor contribution [78]. These findings are similar to reported studies in the literature [35]. The results indicate that $^{\bullet}O_2^-$ and $^{\bullet}OH$ are the main active species for the degradation of RhB by 15-SWCNT/TiO_2 under UV light irradiation, and direct action of hole on TiO_2 played an auxiliary role during the photocatalytic process.

Analysis of the degradation product by GC-Mass analysis confirmed the formation of de-ethylated RhB (*m/z* 415), succinic acid (*m/z* 118), and phenol derivatives (Fig. S10).

3.3.3. Photocatalysis mechanism

The advancement of 15-SWCNT/TiO_2 in photocatalysis should be first attributed to the enhanced adsorptivity which is a prerequisite for good photocatalytic activity [79]. 15-SWCNT-TiO_2 showed the best adsorption strength among the six x-SWCNT/TiO_2 (x = 0.4–15) catalysts (Fig. 8) and the remaining concentration fraction of RhB after dark adsorption on the catalysts obtained from UV–visible absorption spectra verified this assertion. It was obvious that under optimized conditions, after equilibrium in the dark for 30 min, most dye molecules remained in the solution with neat TiO_2 (adsorption 13%) as the catalyst, whereas a large amount of dye molecules was adsorbed (adsorption 52%) on the surface of 15-SWCNT-TiO_2. The higher adsorption by the composite is related to its strong interaction with RhB dye. BET analyses results showed that the synthesized TiO_2, purified SWCNT, and the composite 15-SWCNT-TiO_2 have surface areas of 155 m^2g^{-1}, 303 m^2g^{-1}, and 150 m^2g^{-1}, respectively (Fig. S11). Therefore, high adsorptivity of the composite is not due to higher surface area with respect to neat TiO_2. 15 wt% SWCNT is not enough to increase the composite surface area.

Presence of SWCNT also provided higher light absorption by the composite (Fig. S12). Interestingly, the SWCNT/TiO_2 composite displays an unusual UV–vis spectrum, which almost covered the whole UV–vis region (Fig. S10) and the band gap of the composite is in the visible light range. The band gaps are 3.20 eV and 2.88 eV for neat TiO_2 and 15-SWCNT/TiO_2, respectively (Fig. S12). The Ti-O-C bonds in the composite, similar to carbon-doped TiO_2, contribute in the extension of the absorption light to longer wavelengths. In spite of these findings, the visible-light photocatalytic efficiency of 15-SWCNT/TiO_2 was low. The same result was also reported by others with high intensity visible light [80]. Since the C-introduced levels in the band structure are limited by the amount of C-O-Ti bonds, it is also limited by the amount of the excited electrons, thus the reaction rate is expected to be reduced. It should be recalled that neat TiO_2 does not display any photocatalytic reaction under visible light illumination.

Two distinct contributions from the CNT/TiO_2 composite have been reported. The coupling of the CNTs with TiO_2 creates a rectifying contact that the CNTs act as an electron sink [80]. The strong Ti-O-C/Ti–O(O)C bonds introduce trapping levels in the band gap to the system that could accept photon-excited electrons in the nanocomposites of TiO_2, and as a result suppress the electron/hole pair recombination in CNT/TiO_2 nanocomposites (Scheme 1) [33,81]. The CNT helps to capture photon-excited electrons from the conduction band of the TiO_2 by its large electron-storage capacity. Concurrently, CNT could hinder the recombination of electron-hole pairs by providing fast conduction of the captured photon-excited electrons. The second factor is the electronic configuration of the CNTs; the defects in the CNTs create large numbers of mid band-gap states which aid electronic excitation [80,82]. The effect of the CNT electronic-band structure is higher than the chemical bond between the CNT and TiO_2 in controlling the photocatalysis.

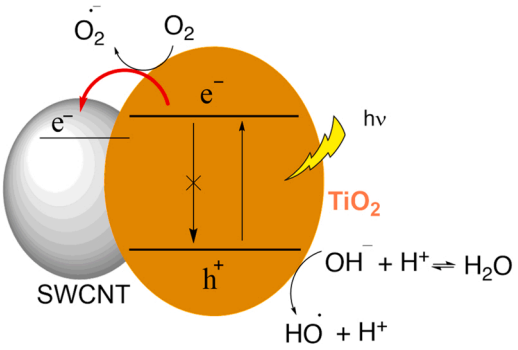

Scheme 1. The proposed mechanism for the photocatalytic performance of 15-SWCNT-TiO_2 in removal of RhB. The CNT could act as electron sinks, i.e., the photogenerated electrons are transferred into the SWCNT providing a low probability of the recombination process.

For evaluating the effects of the purification, the photocatalytic activities of the composites prepared by CNT:TiO_2 weight ratio of 15:100 using purified-SWCNT, crude-SWCNT, and crude-SWCNT with double weight ratio were examined (Fig. 10); they are denoted as 15-SWCNT/TiO_2, 15-(as-synthesized-SWCNT)/TiO_2, and 15-(as-synthesized-2SWCNT)/TiO_2, respectively. In the last composite, the CNT weight was doubled to compensate for its low mass proportion in the composite; the real mass of the SWCNT in the 15%-unpurified-SWCNT is less than 15%-purified-SWCNT because of the presence of MgO and catalysts. Although TEM, TGA, and Raman analysis proved the presence of non-nanotube carbonaceous particles in the purified SWNT-M(j), the effects of the purification on the photocatalytic activity was highly remarkable. It has been well established that TiO_2 is a favorite photocatalyst. However, the limited absorption of light and the high recombination rate of photogenerated electrons (e^-) and positive holes (h^+) decrease its photocatalytic efficiency. To boost the generation of e^-/h^+ by light absorption and reduce their recombination rates, combination of materials such as CNTs or graphene [83] with TiO_2 have been achieved successfully and interesting results obtained. Generally, TiO_2 is used as a bench scale for the quantification of a new photocatalyst activity. Therefore, the photocatalytic activity of a TiO_2-based composite show that recombination rate of photogenerated e^-/h^+ on TiO_2 has been increased or decreased with respect to pure TiO_2. The nanocomposite 15-SWCNT/TiO_2 showed the highest efficiency and removed the RhB almost completely within 120 min. Neat TiO_2 could decompose only 53% of the initial RhB after 120 min. While the adsorption of RhB during 30 min stirring in the dark for 15-(crude-2SWCNT)/TiO_2 and 15-(crude-SWCNT)/TiO_2 was higher

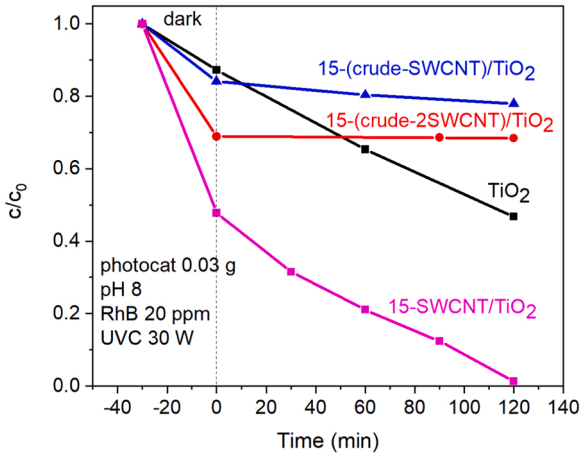

Fig. 10. Effects of the SWCNT purification on the photocatalytic activity of CNT-based nanocomposites for RhB degradation.

than that of TiO_2, their photocatalytic activities were negligible with respect to TiO_2. Comparison of the photocatalytic activities of the SWCNT/TiO_2 composites with that of neat TiO_2, illustrate the boosting effect of the unpurified SWCNT on recombination rate of the photo-generated e^-/h^+ pairs on TiO_2 It is concluded that the presence of the catalyst and support metal impurities in the crude-SWCNT facilitate the electron/hole recombination on the TiO_2 and hence decrease the photocatalytic efficiency of the crude-SWCNT/TiO_2 composite (Fig. 10).

Removing the metal and carbonaceous impurities by HCl-air oxidation-HCl treatments and functionalization of the SWCNT-(j) by HNO_3 reflux both participate in the enhancement of the nanocomposite prepared by the purified-SWCNT/TiO_2. While the formation of Ti-O-C groups on the SWCNT can aid in the photoinduced electron trapping and visible light absorption, the presence of sidewall defects, proven by Raman and XPS, causes significant changes in the SWCNT electronic states and finally in the composite photocatalysis efficiency. The increase of graphitic defects created during the acid oxidation process can also cause a slight improvement in the oxygen reduction activity of CNTs [84]. Our finding is in contrast to that of Xu et al. [85] who reported that the acid treatment decreased the photo-catalytic activity of the titania CNT nano-composites [86].

4. Conclusion

The finding of this study provides a large-scale strategy for the synthesis and purification of SWCNTs. This study presents for the first time the remarkable effects of the purification on the photocatalytic efficiency of SWCNT/TiO_2. SWCNTs were successfully synthesized by catalytic CVD using chemical deposition of CH_4 over FeMo/Al_2O_3 and FeMo/MgO catalysts and the purification of SWCNT-M from the FeMo/MgO catalyst was easily achieved. Of the various acids with different concentrations, reflux time, and temperature that have been examined, the procedure of sequential HCl treatment-air oxidation at 450 °C-second time HCl treatment was efficient for the purification of as-synthesized SWCNT-M. The RhB degradation performance of the 15-SWCNT/TiO_2 nanocomposite was much higher than that of TiO_2 and the composite prepared by unpurified SWCNT. Purification of SWCNT removes the metal catalysts and catalyst-support, improves the retarding effect of SWCNT on photogenerated electron/hole pairs in the composite 15-SWCNT/TiO_2, hence increases its photocatalytic efficiency.

CRediT authorship contribution statement

Sakineh Ghasemzadeh: Carried out the experiments, Writing – original draft. **Hassan Hosseini-Monfared**: Verified the results, supervised the project and Writing – original draft. **Christoph Janiak**: advised, reviewed and edited the article. **Massomeh Ghorbanloo, Thi Hai Yen Beglau**, **Lars Rademacher**, **Alex Spieß** and **Dennis Woschko** carried out characterization analysis.

Declaration of Competing Interest

The authors declare that they have no known competing financial interests or personal relationships that could have appeared to influence the work reported in this paper.

Data Availability

No data was used for the research described in the article.

Acknowledgments

The authors are grateful for financial support of this study by the University of Zanjan, Amirkabir University of Technology, Heinrich-Heine-Universität Düsseldorf, and the Iran National Science Foundation under Grant No. INSF 97009020.

Appendix A. Supplementary material

Supplementary data associated with this article can be found in the online version at doi:10.1016/j.jece.2022.108440.

References

[1] A. Jorio, G. Dresselhaus, M.S. Dresselhaus. Carbon Nanotubes: Advanced Topics in the Synthesis, Structure, Properties and Applications, Springer, 2008.
[2] X. Pan, Z. Fan, W. Chen, Y. Ding, H. Luo, X. Bao, Enhanced ethanol production inside carbon-nanotube reactors containing catalytic particles, Nat. Mater. 6 (2007) 507–511.
[3] M. Ahmad, E. Ahmed, Z. Hong, W. Ahmed, A. Elhissi, N. Khalid, Photocatalytic, sonocatalytic and sonophotocatalytic degradation of Rhodamine B using ZnO/CNTs composites photocatalysts, Ultrason. Sonochem. 21 (2014) 761–773.
[4] S. Kumar, R. Rani, N. Dilbaghi, K. Tankeshwar, K.-H. Kim, Carbon nanotubes: a novel material for multifaceted applications in human healthcare, Chem. Soc. Rev. 46 (2017) 158–196.
[5] S. Qiu, K. Wu, B. Gao, L. Li, H. Jin, Q. Li, Solution-processing of high-purity semiconducting single-walled carbon nanotubes for electronics devices, Adv. Mater. 31 (2019) 1800750.
[6] I. Sanchez Esqueda, X. Yan, C. Rutherglen, A. Kane, T. Cain, P. Marsh, Q. Liu, K. Galatsis, H. Wang, C. Zhou, Aligned carbon nanotube synaptic transistors for large-scale neuromorphic computing, ACS Nano 12 (2018) 7352–7361.
[7] C. Pu, Y. Xu, Q. Liu, A. Zhu, G. Shi, Enantiomers of single chirality nanotube as chiral recognition interface for enhanced electrochemical chiral analysis, Anal. Chem. 91 (2019) 3015–3020.
[8] V. Jourdain, C. Bichara, Current understanding of the growth of carbon nanotubes in catalytic chemical vapour deposition, Carbon 58 (2013) 2–39.
[9] I. Kruusenberg, N. Alexeyeva, K. Tammeveski, J. Kozlova, L. Matisen, V. Sammelselg, J. Solla-Gullón, J.M. Feliu, Effect of purification of carbon nanotubes on their electrocatalytic properties for oxygen reduction in acid solution, Carbon 49 (2011) 4031–4039.
[10] T.-J. Park, S. Banerjee, T. Hemraj-Benny, S.S. Wong, Purification strategies and purity visualization techniques for single-walled carbon nanotubes, J. Mater. Chem. 16 (2006) 141–154.
[11] B. Wu, J. Zhang, Z. Wei, S. Cai, Z. Liu, Chemical alignment of oxidatively shortened single-walled carbon nanotubes on silver surface, J. Phys. Chem. B 105 (2001) 5075–5078.
[12] P. Hou, S. Bai, Q. Yang, C. Liu, H. Cheng, Multi-step purification of carbon nanotubes, Carbon 40 (2002) 81–85.
[13] S.H. Tan, J.C. Goak, S.C. Hong, N. Lee, Purification of single-walled carbon nanotubes using a fixed bed reactor packed with zirconia beads, Carbon 46 (2008) 245–254.
[14] H. Hu, B. Zhao, M.E. Itkis, R.C. Haddon, Nitric acid purification of single-walled carbon nanotubes, J. Phys. Chem. B 107 (2003) 13838–13842.
[15] M. Martınez, M. Callejas, A. Benito, M. Cochet, T. Seeger, A. Anson, J. Schreiber, C. Gordon, C. Marhic, O. Chauvet, Sensitivity of single wall carbon nanotubes to oxidative processing: structural modification, intercalation and functionalisation, Carbon 41 (2003) 2247–2256.
[16] C. Bower, A. Kleinhammes, Y. Wu, O. Zhou, Intercalation and partial exfoliation of single-walled carbon nanotubes by nitric acid, Chem. Phys. Lett. 288 (1998) 481–486.
[17] Y. Yang, H. Zou, B. Wu, Q. Li, J. Zhang, Z. Liu, X. Guo, Z. Du, Enrichment of large-diameter single-walled carbon nanotubes by oxidative acid treatment, J. Phys. Chem. B 106 (2002) 7160–7162.
[18] M.P. de la Flor, R. Camarillo, F. Martínez, C. Jiménez, R. Quiles, J. Rincón, Synthesis and characterization of TiO_2/CNT/Pd: An effective sunlight photocatalyst for neonicotinoids degradation, J. Environ. Chem. Eng. 9 (2021), 106278.
[19] J.O. Olowoyo, M. Kumar, S.L. Jain, J.O. Babalola, A.V. Vorontsov, U. Kumar, Insights into reinforced photocatalytic activity of the CNT–TiO_2 nanocomposite for CO_2 reduction and water splitting, J. Phys. Chem. C 123 (2018) 367–378.
[20] J. Yu, C.Y. Jimmy, M.K.-P. Leung, W. Ho, B. Cheng, X. Zhao, J. Zhao, Effects of acidic and basic hydrolysis catalysts on the photocatalytic activity and microstructures of bimodal mesoporous titania, J. Catal. 217 (2003) 69–78.
[21] J.I. Langford, A. Wilson, Scherrer after sixty years: a survey and some new results in the determination of crystallite size, J. Appl. Crystallogr 11 (1978) 102–113.
[22] A.R. Harutyunyan, B.K. Pradhan, U. Kim, G. Chen, P. Eklund, CVD synthesis of single wall carbon nanotubes under “soft” conditions, Nano Lett. 2 (2002) 525–530.
[23] Z. Niu, Y. Fang, Effects of synthesis time for synthesizing single-walled carbon nanotubes over Mo–Fe–MgO catalyst and suggested growth mechanism, J. Cryst. Growth 297 (2006) 228–233.
[24] B. Zheng, Y. Li, J. Liu, CVD synthesis and purification of single-walled carbon nanotubes on aerogel-supported catalyst, Appl. Phys. A 74 (2002) 345–348.
[25] G. Boskovic, S. Ratkovic, E. Kiss, O. Geszti, Carbon nanotubes purification constrains due to large Fe–Ni/Al_2O_3 catalyst particles encapsulation, Bull. Mater. Sci. 36 (2013) 1–7.
[26] Y. Chen, L. Wei, B. Wang, S. Lim, D. Ciuparu, M. Zheng, J. Chen, C. Zoican, Y. Yang, G.L. Haller, Low-defect, purified, narrowly (n, m)-dispersed single-walled

carbon nanotubes grown from cobalt-incorporated MCM-41, ACS Nano 1 (2007) 327–336.
[27] M. Karimi Estahbanati, M. Feilizadeh, M. Shokrollahi Yancheshmeh, M.C. Iliuta, Effects of carbon nanotube and carbon sphere templates in TiO_2 composites for photocatalytic hydrogen production, Ind. Eng. Chem. Res. 58 (2019) 2770–2783.
[28] H. Zhang, X. Lv, Y. Li, Y. Wang, J. Li, P25-graphene composite as a high performance photocatalyst, ACS Nano 4 (2010) 380–386.
[29] F. Avilés, J. Cauich-Rodríguez, L. Moo-Tah, A. May-Pat, R. Vargas-Coronado, Evaluation of mild acid oxidation treatments for MWCNT functionalization, Carbon 47 (2009) 2970–2975.
[30] R. Matjie, M. Scurrell, J. Bunt, The selective dissolution of alumina, cobalt and platinum from a calcined spent catalyst using different lixiviants, Miner. Eng. 18 (2005) 801–810.
[31] A.R. Biris, E. Dervishi, S. Simon, D. Lupu, I. Misan, C. Iancu, S.V. Clichici, Y. Xu, F. Watanabe, A.S. Biris, Analytic studies of high quality singlewall carbon nanotubes synthesized on a novel Fe: Mo: MgO catalyst, Phys. E Low-Dimens. Syst. Nanostruct. 43 (2010) 552–558.
[32] A.C. Dillon, T. Gennett, K.M. Jones, J.L. Alleman, P.A. Parilla, M.J. Heben, A simple and complete purification of single-walled carbon nanotube materials, Adv. Mater. 11 (1999) 1354–1358.
[33] K. Woan, G. Pyrgiotakis, W. Sigmund, Photocatalytic carbon-nanotube–TiO_2 composites, Adv. Mater. 21 (2009) 2233–2239.
[34] Y. Yu, C.Y. Jimmy, J.-G. Yu, Y.-C. Kwok, Y.-K. Che, J.-C. Zhao, L. Ding, W.-K. Ge, P.-K. Wong, Enhancement of photocatalytic activity of mesoporous TiO_2 by using carbon nanotubes, Appl. Catal. A Gen. 289 (2005) 186–196.
[35] L. Ling, C. Wang, M. Ni, C. Shang, Enhanced photocatalytic activity of TiO_2/single-walled carbon nanotube (SWCNT) composites under UV-A irradiation, Sep. Purif. Technol. 169 (2016) 273–278.
[36] M.-Q. Yang, N. Zhang, Y.-J. Xu, Synthesis of fullerene–, carbon nanotube–, and graphene–TiO_2 nanocomposite photocatalysts for selective oxidation: a comparative study, ACS Appl. Mater. Interfaces 5 (2013) 1156–1164.
[37] S. Liu, N. Zhang, Z.-R. Tang, Y.-J. Xu, Synthesis of one-dimensional CdS@ TiO_2 core–shell nanocomposites photocatalyst for selective redox: the dual role of TiO_2 shell, ACS Appl. Mater. Interfaces 4 (2012) 6378–6385.
[38] B. Abramović, V. Despotović, D. Šojić, N. Finčur, Mechanism of clomazone photocatalytic degradation: hydroxyl radical, electron and hole scavengers, React. Kinet. Mech. Catal. 115 (2015) 67–79.
[39] R. Philippe, A. Morançais, M. Corrias, B. Caussat, Y. Kihn, P. Kalck, D. Plee, P. Gaillard, D. Bernard, P. Serp, Catalytic production of carbon nanotubes by fluidized-bed CVD, Chem. Vap. Depos. 13 (2007) 447–457.
[40] C. Journet, W.K. Maser, P. Bernier, A. Loiseau, M. Lamy de La Chapelle, S. Lefrant, P. Deniard, R. Lee, J.E. Fischer, Large-scale production of single-walled carbon nanotubes by the electric-arc technique, Nature, 388, 1997, pp. 756–758.
[41] J. Kong, A.M. Cassell, H. Dai, Chemical vapor deposition of methane for single-walled carbon nanotubes, Chem. Phys. Lett. 292 (1998) 567–574.
[42] S. Lyu, B. Liu, S. Lee, C. Park, H. Kang, C. Yang, C.J. Lee, Large-scale synthesis of high-quality single-walled carbon nanotubes by catalytic decomposition of ethylene, J. Phys. Chem. B 108 (2004) 1613–1616.
[43] H. Yan, Q. Li, J. Zhang, Z. Liu, Possible tactics to improve the growth of single-walled carbon nanotubes by chemical vapor deposition, Carbon 40 (2002) 2693–2698.
[44] H. Ago, K. Nakamura, N. Uehara, M. Tsuji, Roles of metal− support interaction in growth of single-and double-walled carbon nanotubes studied with diameter-controlled iron particles supported on MgO, J. Phys. Chem. B 108 (2004) 18908–18915.
[45] K. MacKenzie, O. Dunens, A.T. Harris, A review of carbon nanotube purification by microwave assisted acid digestion, Sep. Purif. Technol. 66 (2009) 209–222.
[46] B. Liu, S. Lyu, S. Jung, H. Kang, C.-W. Yang, J. Park, C. Park, C.J. Lee, Single-walled carbon nanotubes produced by catalytic chemical vapor deposition of acetylene over Fe–Mo/MgO catalyst, Chem. Phys. Lett. 383 (2004) 104–108.
[47] Q. Wu, L. Qiu, L. Zhang, H. Liu, R. Ma, P. Xie, R. Liu, P. Hou, F. Ding, C. Liu, Temperature-dependent selective nucleation of single-walled carbon nanotubes from stabilized catalyst nanoparticles, Chem. Eng. J. 431 (2022), 133487.
[48] P.-X. Hou, C. Liu, H.-M. Cheng, Purification of carbon nanotubes, Carbon 46 (2008) 2003–2025.
[49] K. Tohji, T. Goto, H. Takahashi, Y. Shinoda, N. Shimizu, B. Jeyadevan, I. Matsuoka, Y. Saito, A. Kasuya, T. Ohsuna, Purifying single-walled nanotubes, Nature 383 (1996), 679-679.
[50] Y. Li, X. Zhang, J. Luo, W. Huang, J. Cheng, Z. Luo, T. Li, F. Liu, G. Xu, X. Ke, Purification of CVD synthesized single-wall carbon nanotubes by different acid oxidation treatments, Nanotechnology 15 (2004) 1645.
[51] J. Ma, J.N. Wang, Purification of single-walled carbon nanotubes by a highly efficient and nondestructive approach, Chem. Mater. 20 (2008) 2895–2902.
[52] J. Liu, A.G. Rinzler, H. Dai, J.H. Hafner, R.K. Bradley, P.J. Boul, A. Lu, T. Iverson, K. Shelimov, C.B. Huffman, Fullerene pipes, Science 280 (1998) 1253–1256.
[53] D. Tasis, N. Tagmatarchis, A. Bianco, M. Prato, Chemistry of carbon nanotubes, Chem. Rev. 106 (2006) 1105–1136.
[54] K. Balasubramanian, M. Burghard, Chemically functionalized carbon nanotubes, Small 1 (2005) 180–192.
[55] S.Y. Chew, S.H. Ng, J. Wang, P. Novák, F. Krumeich, S.L. Chou, J. Chen, H.K. Liu, Flexible free-standing carbon nanotube films for model lithium-ion batteries, Carbon 47 (2009) 2976–2983.
[56] A. Thess, R. Lee, P. Nikolaev, H. Dai, P. Petit, J. Robert, C. Xu, Y.H. Lee, S.G. Kim, A.G. Rinzler, Crystalline ropes of metallic carbon nanotubes, Science 273 (1996) 483–487.
[57] E. Lamouroux, P. Serp, P. Kalck, Catalytic routes towards single wall carbon nanotubes, Catal. Rev. 49 (2007) 341–405.
[58] S.K. Pillai, S.S. Ray, M. Moodley, Purification of single-walled carbon nanotubes, J. Nanosci. Nanotechnol. 7 (2007) 3011–3047.
[59] K. Kinoshita, Carbon: Electrochemical and Physicochemical Properties, 1988.
[60] J.L. Zimmerman, R.K. Bradley, C.B. Huffman, R.H. Hauge, J.L. Margrave, Gas-phase purification of single-wall carbon nanotubes, Chem. Mater. 12 (2000) 1361–1366.
[61] A. Rinzler, J. Liu, H. Dai, P. Nikolaev, C. Huffman, F. Rodriguez-Macias, P. Boul, A. H. Lu, D. Heymann, D. Colbert, Large-scale purification of single-wall carbon nanotubes: process, product, and characterization, Appl. Phys. A Mater. Sci. Process. 67 (1998).
[62] A.M. Rao, E. Richter, S. Bandow, B. Chase, P. Eklund, K. Williams, S. Fang, K. Subbaswamy, M. Menon, A. Thess, Diameter-selective Raman scattering from vibrational modes in carbon nanotubes, Science 275 (1997) 187–191.
[63] T. Belin, F. Epron, Characterization methods of carbon nanotubes: a review, Mater. Sci. Eng. B 119 (2005) 105–118.
[64] T. Yamabe, K. Fukui, The Science and Technology of Carbon Nanotubes, Elsevier, 1999.
[65] N.I. Kovtyukhova, T.E. Mallouk, L. Pan, E.C. Dickey, Individual single-walled nanotubes and hydrogels made by oxidative exfoliation of carbon nanotube ropes, J. Am. Chem. Soc. 125 (2003) 9761–9769.
[66] A. Kukovecz, C. Kramberger, M. Holzinger, H. Kuzmany, J. Schalko, M. Mannsberger, A. Hirsch, On the stacking behavior of functionalized single-wall carbon nanotubes, J. Phys. Chem. B 106 (2002) 6374–6380.
[67] E. Mickelson, C. Huffman, A. Rinzler, R. Smalley, R. Hauge, J. Margrave, Fluorination of single-wall carbon nanotubes, Chem. Phys. Lett. 296 (1998) 188–194.
[68] P. Puech, E. Flahaut, A. Bassil, T. Juffmann, F. Beuneu, W. Bacsa, Raman bands of double-wall carbon nanotubes: comparison with single-and triple-wall carbon nanotubes, and influence of annealing and electron irradiation, J. Raman Spectrosc. 38 (2007) 714–720.
[69] S. Utsumi, H. Honda, Y. Hattori, H. Kanoh, K. Takahashi, H. Sakai, M. Abe, M. Yudasaka, S. Iijima, K. Kaneko, Direct evidence on C− C single bonding in single-wall carbon nanohorn aggregates, J. Phys. Chem. C 111 (2007) 5572–5575.
[70] P.-C. Wang, Y.-C. Liao, Y.-L. Lai, Y.-C. Lin, C.-Y. Su, C.-H. Tsai, Y.-J. Hsu, Conversion of pristine and p-doped sulfuric-acid-treated single-walled carbon nanotubes to n-type materials by a facile hydrazine vapor exposure process, Mater. Chem. Phys. 134 (2012) 325–332.
[71] A. Fujishima, T.N. Rao, D.A. Tryk, Titanium dioxide photocatalysis, J. Photochem. Photobiol. C Photochem. Rev. 1 (2000) 1–21.
[72] Y. Gao, Y. Masuda, Z. Peng, T. Yonezawa, K. Koumoto, Room temperature deposition of a TiO2 thin film from aqueous peroxotitanate solution, J. Mater. Chem. 13 (2003) 608–613.
[73] S. Sakthivel, H. Kisch, Daylight photocatalysis by carbon-modified titanium dioxide, Angew. Chem. Int. Ed. 42 (2003) 4908–4911.
[74] F. Chen, Q. Yang, Y. Zhong, H. An, J. Zhao, T. Xie, Q. Xu, X. Li, D. Wang, G. Zeng, Photo-reduction of bromate in drinking water by metallic Ag and reduced graphene oxide (RGO) jointly modified BiVO4 under visible light irradiation, Water Res. 101 (2016) 555–563.
[75] Y. Chen, Z. Xiang, D. Wang, J. Kang, H. Qi, Effective photocatalytic degradation and physical adsorption of methylene blue using cellulose/GO/TiO_2 hydrogels, RSC Adv. 10 (2020) 23936–23943.
[76] D. Chaudhary, N. Khare, V. Vankar, Ag nanoparticles loaded TiO_2/MWCNT ternary nanocomposite: a visible-light-driven photocatalyst with enhanced photocatalytic performance and stability, Ceram. Int. 42 (2016) 15861–15867.
[77] Y. Zhang, N. Zhang, Z.-R. Tang, Y.-J. Xu, Graphene transforms wide band gap ZnS to a visible light photocatalyst. The new role of graphene as a macromolecular photosensitizer, ACS Nano 6 (2012) 9777–9789.
[78] M.S. Dorraji, A. Amani-Ghadim, M. Rasoulifard, S. Taherkhani, H. Daneshvar, The role of carbon nanotube in zinc stannate photocatalytic performance improvement: experimental and kinetic evidences, Appl. Catal. B Environ. 205 (2017) 559–568.
[79] W. Morales, M. Cason, O. Aina, N.R. de Tacconi, K. Rajeshwar, Combustion synthesis and characterization of nanocrystalline WO_3, J. Am. Chem. Soc. 130 (2008) 6318–6319.
[80] G. Pyrgiotakis, S.-H. Lee, W. Sigmund, Advanced photocatalysis with anatase nano-coated multi-walled carbon nanotubes, MRS Online Proc. Libr. (OPL) 876, 2005.
[81] V.R. Djokić, A.D. Marinković, M. Mitrić, P.S. Uskoković, R.D. Petrović, V. R. Radmilović, D.T. Janaćković, Preparation of TiO_2/carbon nanotubes photocatalysts: the influence of the method of oxidation of the carbon nanotubes on the photocatalytic activity of the nanocomposites, Ceram. Int. 38 (2012) 6123–6129.
[82] R. Leary, A. Westwood, Carbonaceous nanomaterials for the enhancement of TiO_2 photocatalysis, Carbon 49 (2011) 741–772.
[83] L. Yang, Y. Luo, L. Yang, S. Luo, X. Luo, W. Dai, T. Li, Y. Luo, Enhanced photocatalytic activity of hierarchical titanium dioxide microspheres with combining carbon nanotubes as “e-bridge, J. Hazard. Mater. 367 (2019) 550–558.
[84] E.J. Biddinger, U.S. Ozkan, Role of graphitic edge plane exposure in carbon nanostructures for oxygen reduction reaction, J. Phys. Chem. C 114 (2010) 15306–15314.
[85] Y.-J. Xu, Y. Zhuang, X. Fu, New insight for enhanced photocatalytic activity of TiO_2 by doping carbon nanotubes: a case study on degradation of benzene and methyl orange, J. Phys. Chem. C 114 (2010) 2669–2676.
[86] N. Hintsho, L. Petrik, A. Nechaev, S. Titinchi, P. Ndungu, Photo-catalytic activity of titanium dioxide carbon nanotube nano-composites modified with silver and palladium nanoparticles, Appl. Catal. B Environ. 156 (2014) 273–283.